ACS OMEGA

Open Access

http://pubs.acs.org/journal/acsodf

Article

Integrating CRISPR-Cas12a with Aptamer as a Logic Gate Biosensing Platform for the Detection of CD33 and CD123

Xinyi Yang, Xiaolong Shi, Chenyu Lv, Wenbin Liu, Fengyue Zhang,* and Bo Liu*

Cite This: *ACS Omega* 2025, 10, 13634−13644

Read Online

ACCESS | Metrics & More | Article Recommendations | Supporting Information

ABSTRACT: Molecular logic gates, as biomolecule-based computational systems, are highly suitable for multitarget detection due to their programmability and modularity. However, existing systems are primarily limited to nucleic acid detection and have not been widely applied to disease-related sensing, particularly for disease antigens. CD33 and CD123 are critical biomarkers for acute myeloid leukemia (AML), yet conventional detection methods rely on expensive equipment and complex procedures, limiting their accessibility and practicality. This study designs a DNA logic gate system integrating nucleic acid aptamers, catalytic hairpin assembly (CHA), and CRISPR-Cas12a, pioneering its use for AML antigen detection. The system comprises three modules: input recognition, signal amplification, and signal transduction. Nucleic acid aptamers specifically identify CD33 and CD123, while CHA enables efficient signal amplification and CRISPR-Cas12a generates a fluorescent output via trans-cleavage activity. The system operates stably at room temperature and implements multiple logic gate models, including YES, OR, AND, NOR, and INHIBIT, enabling the simultaneous detection of CD33 and CD123. Experimental results are visually distinguishable under blue light, and the system requires only standard fluorescence detection instruments. In serum samples, it exhibits excellent selectivity and stability, with a detection limit of 0.5 ng/mL. This study pioneers the application of logic gate technology for disease antigen detection, addressing a critical gap in AML biomarker sensing. Our study indicates that this logic detection platform, characterized by its simplicity in operation, high sensitivity, and versatility in logic functions, holds promise as a potent sensing system for the intelligent multiplex target detection of disease antigens, environmental pollutants, and heavy metals.

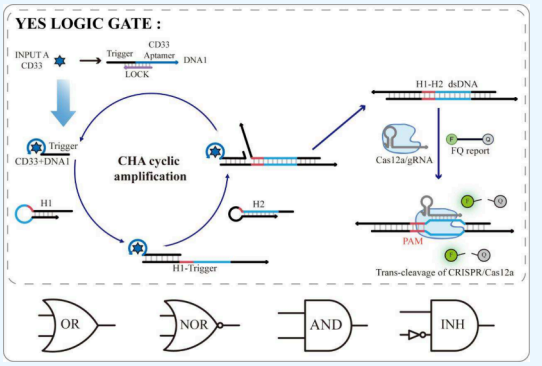

1. INTRODUCTION

Molecular logic gates represent a computational and signal processing approach based on biochemical or chemical molecular reactions, particularly suitable for multi-input detection, as they can simultaneously respond to multiple signal inputs, enabling parallel analysis of complex biomarkers. These gates mimic traditional microprocessors to execute Boolean functions for information processing. Typically, the presence or absence of inputs and outputs is encoded using 1 and 0.[1] Strand displacement,[2−4] hairpin assembly,[5,6] DNAzymes,[7,8] and other DNA-based computational logic gates[9] have all been created and described. Most of these gates rely on base pairing or DNAzyme-catalyzed DNA cleavage. Currently, there are few studies using disease antigens as inputs for molecular logic gates. In this study, we designed a DNA logic gate based on catalytic hairpin assembly (CHA) and CRISPR, which is regulated by the binding of the aptamer to the antigen protein.

Acute myeloid leukemia (AML) is a common hematologic cancer in adults, with CD123 and CD33 coexpressed on over 95% of AML cells, including leukemia stem cells. These antigens are crucial for diagnosis, prognosis, and treatment.[10] Traditional detection methods, such as flow cytometry, ELISA, and immunohistochemistry,[11−14] require expensive equipment, complex procedures, and long processing times. Therefore, there is a need for simpler, cost-effective methods with high specificity for detecting AML-specific antigens. In this study, we selected CD33 and CD123 as targets for the logic gate model to evaluate its performance.[15−17]

Aptamers are short nucleic acids or peptides obtained from synthetic libraries using exponential enrichment techniques (SELEX).[18,19] Due to their unique three-dimensional structures, they exhibit high binding and selectivity for specific target molecules. Since the discovery of aptamers in 1990, numerous scientists have identified a variety of aptamers that can bind to various targets, including proteins, metal ions, cells, bacteria, viruses, and organic and inorganic small molecules.[20,21] Aptamers are widely used in bioanalysis because of

Received: January 22, 2025
Revised: March 5, 2025
Accepted: March 20, 2025
Published: March 26, 2025

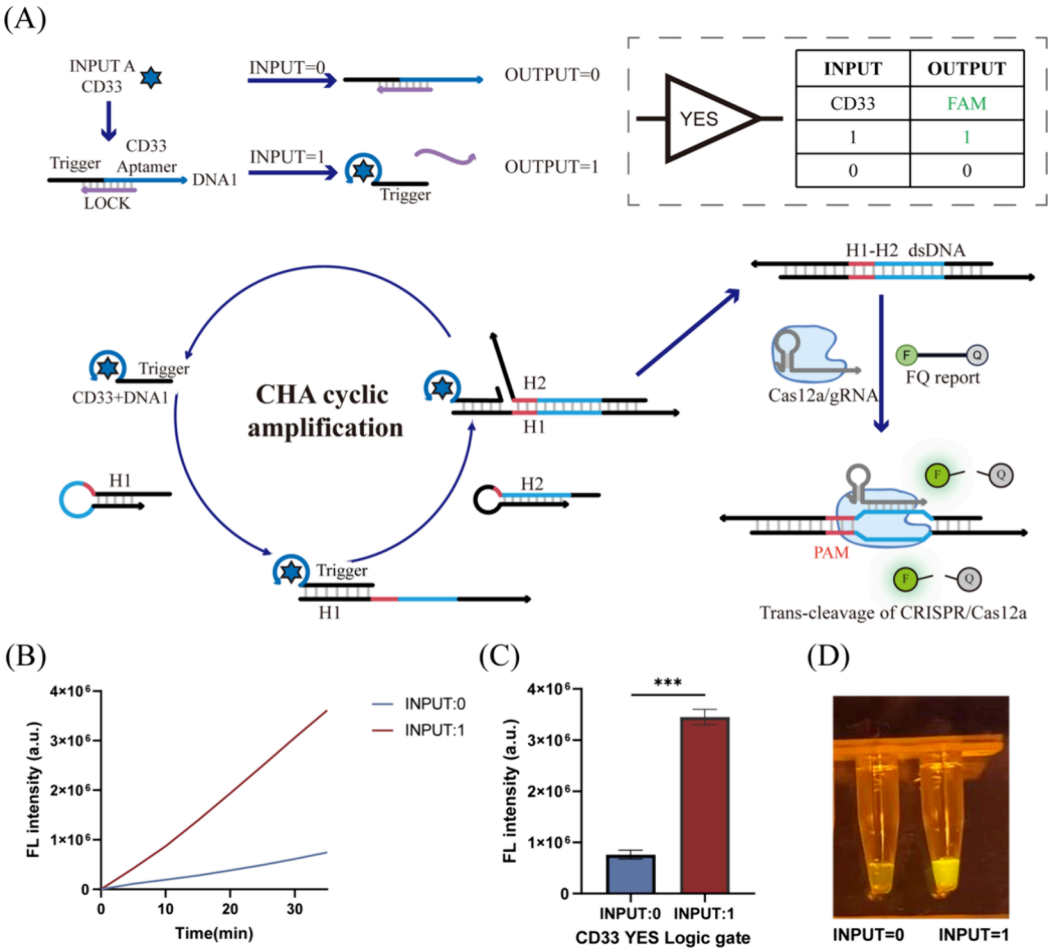

Figure 1. Operating principle and experimental results of the YES logic gate: (A) Schematic representation of the YES gate with CD33 as input. The 100 nM aptamer (DNA1) was used to recognize the input. Two hairpin probes (500 nM H1 and 500 nM H2) were used to assemble H1/H2 dsDNA. The 150 nM Cas12a/gRNA complex was used to cleave the 1 μM FQ reporter (modified with BHQ and FAM) to obtain the fluorescence output. Inset: The truth table of the YES logic gate. CD33:50 ng/mL. (B) Real-time fluorescence curves of CRISPR-CHA reaction in YES logic gate. (C) Fluorescence intensity of YES logic gate. Statistical significance was determined by *t* test (***$p < 0.001$, $n = 3$). (D) Color reaction under blue light.

their wide detection range, chemical stability, low synthetic cost, and high binding affinity, making them valuable tools for molecular recognition.[22,23] To expand the spectrum of potential drivers for DNA logic gates, the process of binding nucleic acid aptamers to recognize antigenic proteins is used as an input.

Catalytic hairpin assembly (CHA) is a unique target recycling amplification technique that utilizes single-stranded DNA (ssDNA) to trigger the cross-opening of two DNA hairpins, producing a large number of double-stranded DNA (dsDNA) outputs.[24,25] This method is characterized by its ability to amplify signals, maintain low background noise, and facilitate straightforward operation and design.[26,27] As a sequence-specific signal transduction and amplification tool, CHA has been widely applied in isothermal nucleic acid amplification, sensing, and detection.[28,29] A single CHA response, however, often suffers from insufficient gain and lower sensitivity. This limitation can be improved by combining CHA with other signal amplification strategies.

The CRISPR-Cas system, comprising clustered regularly interspaced short palindromic repeats (CRISPR) and CRISPR-associated (Cas) proteins, has emerged as a groundbreaking technology in the biological sciences and has been widely adopted as a powerful signal amplification tool in molecular diagnostics.[30−32] Cas13a, Cas12a, Cas12b, and Cas14 are examples of class 2 type V and VI Cas proteins that were recently found to exhibit collateral cleavage activity, which holds promising for highly sensitive nucleic acid detection.[33−37] Specifically, CRISPR-Cas12a (Cpf1) is a type of CRISPR-Cas system composed of guide RNA (gRNA) and Cas12a nuclease. Upon recognition of the protospacer adjacent motif (PAM) (5′-TTTN-3′) site in double-stranded DNA (dsDNA), Cas12a is activated.[38,39] Activated CRISPR-Cas12a can not only cleave the double-stranded target DNA (cis-cleavage) but also indiscriminately cleave single-stranded DNA (trans-cleavage). This property endows the CRISPR-Cas12a system with great potential for the design of biosensors, including fluorescence detectors,[40−42] colorimetric biosensors,[43,44] and lateral flow strips.[45−47]

In this study, we developed a universal molecular logic gate model by integrating CRISPR-Cas12a as a signal transduction tool with aptamers and catalytic hairpins, enabling intelligent protein detection and expanding the range of logic gate inputs. Using CD33, a specific antigen for AML, and CD123 as dual inputs, we combined nucleic acid aptamer recognition with the signal amplification capabilities of CHA and CRISPR-Cas12a,

https://doi.org/10.1021/acsomega.5c00660
ACS Omega 2025, 10, 13634−13644

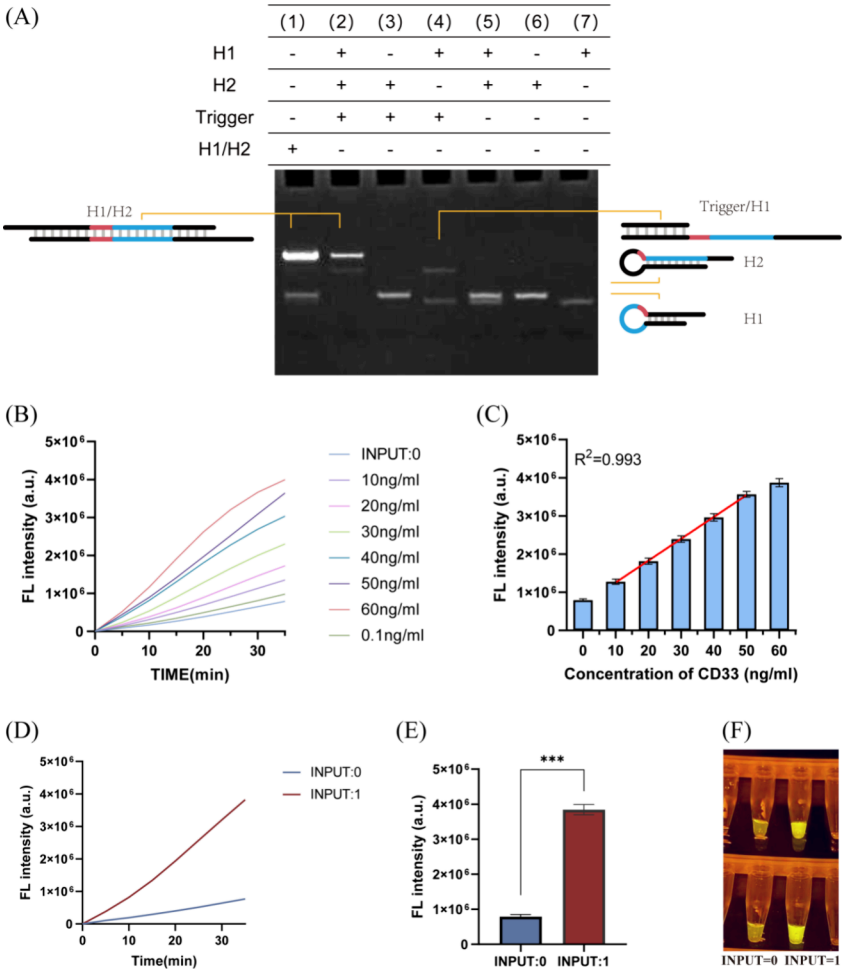

Figure 2. Analytical performance of the YES logic gate: (A) PAGE results: Confirm the assembly process between Trigger, H1 and H2 in YES logic gate under different conditions. H1:500 nM; H2:500 nM; Trigger: 100 nM; H1/H2:500 nM. (B) Real-time fluorescence of CRISPR-CHA with varying CD33 concentrations. (C) The linear range for CD33 analysis. (D) Real-time fluorescence graph of the CRISPR-CHA of the YES logic gate in serum samples. (E) Fluorescence intensity of YES logic gate in serum sample. Statistical significance was determined by *t* test (***$p < 0.001$, $n = 3$). (F) Color reaction under blue light. Concentrations of DNA1/LOCK1:100 nM, H1 and H2:0.5 μM, CD33 and CD123:50 ng/mL were incubated for 55 min, followed by the addition of Cas12a/gRNA: 150 nM, FQ reporter: 1 μM.

generating a strong fluorescence signal to represent logical operations. Leveraging the programmable nature of DNA, we designed and constructed DNA probes, ultimately creating a biosensor platform capable of implementing YES, OR, AND, INHIBIT, and NOR logic gates.

2. EXPERIMENTAL SECTION

2.1. Materials and Reagents. Chemicals and Materials. All of the HPLC-purified DNA probes were purchased from Sangon Biotech Co., Ltd. (Shanghai, China) Tables S1−S7 (Supporting Information) contains a list of their sequences. The aptamer sequences used in this study were obtained from previous studies CD33[15] and CD123,[16] where they were originally identified and validated through SELEX. CD33 and CD123 were purchased from Sangon Biotech Co., Ltd. (Shanghai, China). 10× NEBuffer r2.1 and EnGen Lba Cas12a (Cpf1) were acquired from New England Biolabs Ltd. (Whitby, ON, Canada). Human AB Serum was purchased from GeminiBio, Ltd. (California, USA). Other reagents were of analytical grade and were purchased from Sangon Biotech Co., Ltd. (Shanghai, China). Direct-Q8UV-R was used to prepare the buffer.

2.2. Logic Computing Operations. A 20 mM Tris-HCl buffer (pH 7.5, 140 mM NaCl, 5 mM KCl, and 12.5 mM $MgCl_2$) was used to dissolve each DNA probe. The Cas12a was dissolved in 1× NEBuffer r2.1. Diethyl pyrocarbonate (DEPC) treated water was used to prepare the gRNA and FQ reporter solution.

The aim was to create a hairpin structure by annealing H1 and H2. The samples were heated to 95 °C for ten min and then cooled to room temperature as part of the annealing process. After being annealed, the hairpin DNA was kept in storage at 4 °C.

In the YES logic gate, at room temperature, 200 nM LOCK and 100 nM DNA1 were incubated for 15 min. After adding 50 ng/mL CD33, 500 nM H1, and 500 nM H2, the mixture was incubated at room temperature for 55 min. After adding 150 nM Cas12a, 200 nM gRNA, and 1 μM FQ reporter, the mixture was incubated for 35 min at 25 °C. Using the Applied Biosystems QuantStudio 3, fluorescence values were recorded at 15 s intervals, and the ensuing kinetics were noted.

The inputs of the OR, AND, and INHIBIT logic gates were 50 ng/mL of CD33 and CD123; 100 nM DNA2 and 200 nM LOCK2 containing CD123 aptamer sequences were added, and an extra 80 nM Trigger was needed in the NOR logic gate.

https://doi.org/10.1021/acsomega.5c00660
ACS Omega 2025, 10, 13634−13644

The YES logic gate's other processes were the same. The images were taken using an iPad fitted with a wide camera, and the logic results were visible to the naked eye in BLUE light.

2.3. Polyacrylamide Gel Electrophoresis (PAGE) Analysis. The details of the PAGE procedures were listed in the Supporting Information. The experimental results of the feasibility of the logic gates analyzed using Polyacrylamide Gel Electrophoresis (PAGE) are shown in Figure S1.

2.4. Analysis of CD33 in the Serum Sample. The serum samples were centrifuged at 4 °C and 3000 rpm for 10 min, and 50 μL of the supernatant was mixed with 50 μL of DEPC water and heated at 75 °C for 10 min to inactivate the deoxyribonuclease. We added different concentrations of CD33 to healthy human serum to determine the feasibility of the logic gate model in the serum environment and investigate the effect of the serum matrix.

3. RESULTS AND DISCUSSION

3.1. YES Logic Gate. *3.1.1. Design of "YES Logic Gate"-Based Structure.* Figure 1 schematically shows the YES logic gate based on CHA and CRISPR-Cas12a (sequences are given in Table S1). Using CD33 as a model target, we first created a YES logic gate. The output fluorescence intensity is expressed as 1 or 0.

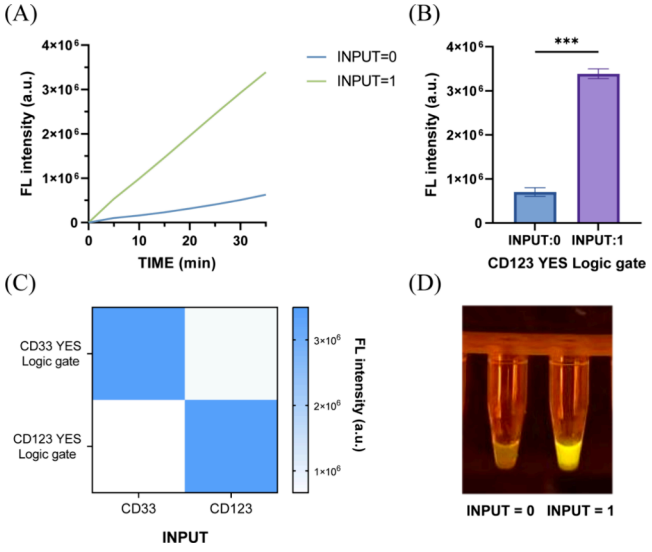

Figure 3. YES gate with CD123 as input: (A) Real-time fluorescence curves of the CRISPR-CHA reaction in the YES logic gate. (B) Fluorescence intensity of the YES logic gate. Statistical significance was determined by *t* test (***$p < 0.001$, $n = 3$). (C) Orthogonality Analysis of the YES Logic Gate. (D) Color reaction under blue light. Concentrations of DNA1/LOCK1:100 nM, H1 and H2:0.5 μM, CD33 and CD123:50 ng/mL were incubated for 55 min, followed by the addition of Cas12a/gRNA: 150 nM, FQ reporter: 1 μM.

Table 1. Detection of CD33 in Human Serum Using a YES Logic Gate

sample	add (ng/mL)	founded (ng/mL)	recovery (%)	RSD[a] (%)
1	20	18.74	93.72	5.50
2	30	29.71	99.03	3.30
3	40	43.39	108.47	2.73

[a]RSD: the relative standard deviation.

The LOCK probe blocks the CD33 aptamer sequence and the Trigger DNA sequence in DNA1 in the duplex. By forming the CD33-aptamer complex, the target CD33 can open the duplex structure, releasing the 3′ end of the Trigger DNA. Through toehold-mediated strand displacement, the 3′ end of the trigger binds to the 5′ end of hairpin probe 1 (H1). The exposed 3′-overhang in H1 then serves as a new toehold to open hairpin probe 2 (H2), forming the H1/H2 duplex and releasing Trigger. Afterward, the Trigger can be recycled to activate additional H1 and H2, producing a large amount of H1−H2 dsDNA. The crRNA aids CRISPR-Cas12a in identifying the protospacer sequence and PAM site in H1−H2 dsDNA. ssDNA engineered with BHQ and FAM can be cleaved by activated Cas12a to produce a strong fluorescence signal that can be used to track logic functions. The real-time fluorescence curves of the CRISPR-Cas12a and CHA reaction mixture (CRISPR-CHA) are shown in Figure 1B. LOCK DNA blocked the Trigger domain when CD33 was not present. There can be no CHA reaction between H1 and H2. As a result, only the background fluorescence signal is discernible.

The logic outcomes can be directly observed under blue light transillumination (Figure 1D). As shown in Figure 1, an input of 1 produces an output of 1, while an input of 0 results in an output of 0. The final fluorescence intensity of the YES logic gate is presented in Figure 1C, where an input of 1 generates a strong fluorescent signal, showing a statistically significant difference ($p < 0.001$, $n = 3$) compared to the control group with an input of 0.

3.1.2. Feasibility and Selectivity Investigation. In the YES logic gate, signal amplification and conversion are critical, which are achieved through the coupling of the CHA and CRISPR-Cas systems. To verify its feasibility, PAGE was employed to confirm the CHA reaction, with the experimental results shown in Figure 2A. The fluorescence experiments were conducted to demonstrate that the enhancement of the output signal was specifically due to the addition of CD33, rather than other components, as illustrated in Figure S2.

The two hairpin probes (H1 and H2) are located in lanes 7 and 6, and the annealed H1/H2 dsDNA is in lane 1 in Figure 2A. A new H1/H2 duplex band shows up in lane 2 following Trigger's addition, indicating that Trigger successfully started the CHA. Conversely, when Trigger is absent from lane 5, no band for the H1/H2 duplex is seen. Trigger only reacts with H1 because adding Trigger and H1 results in a Trigger/H1 hybridization chain in lane 4, while adding Trigger and H2 does not result in a reaction in lane 3. These results successfully confirmed the assembly reaction between H1, H2 and Trigger.

Another important aspect is the specificity. To ensure that the logic gate would generate outputs only for the right target molecule, we compared CD33 to the other common antigens in AML disease, such as CD123 and CD34. As shown in Figure S2, the logic gate demonstrated efficacy only against CD33 and no interference from other antigens. These results demonstrated the high selectivity and good specificity of this YES logic gate for target input detection. Using specific antigens as detection targets is more targeted than detecting gene mutation sites and reduces false-positive and false-negative results.

3.1.3. Analytical Performance. Several experimental parameters, including reaction temperature (Figure S3), CRISPR incubation time (Figure S4), and probe sequences

https://doi.org/10.1021/acsomega.5c00660
ACS Omega 2025, 10, 13634−13644

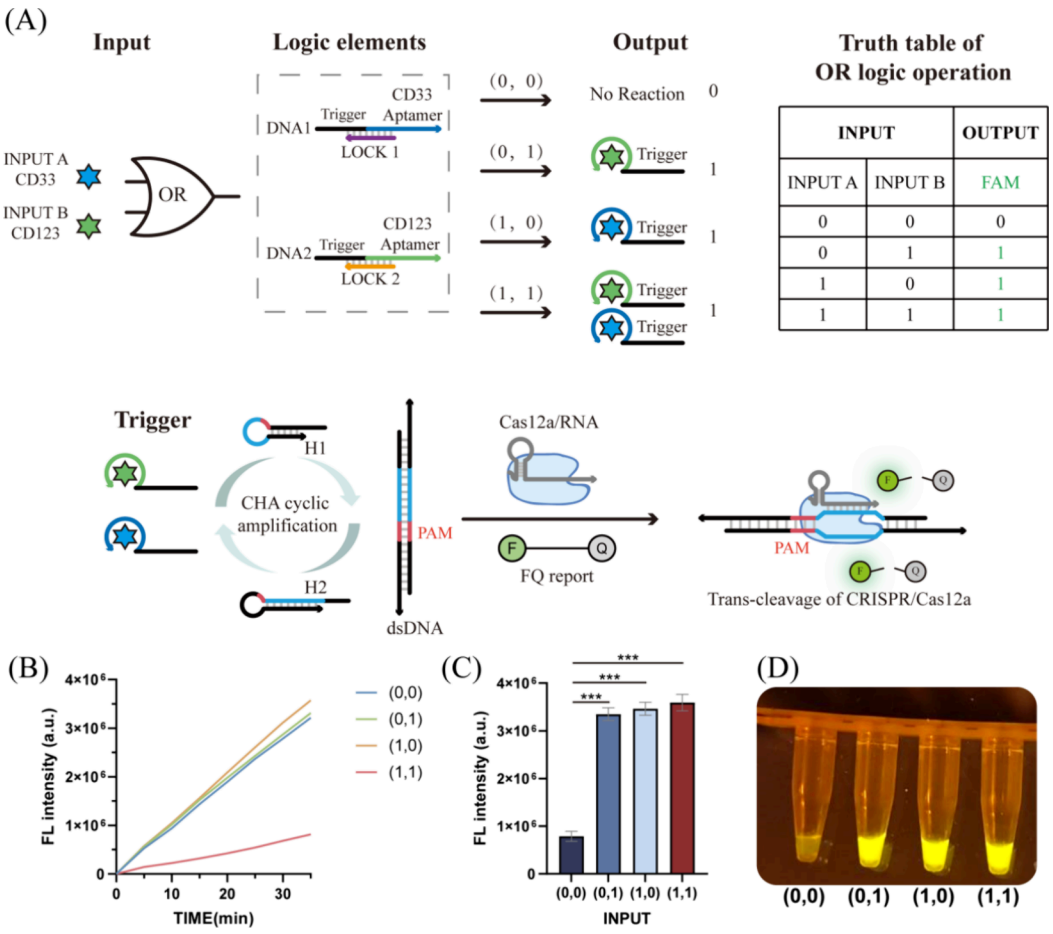

Figure 4. Operating principle and experimental results of the OR logic gate: (A) Schematic illustration of the OR logic gate using CD33 and CD123 as inputs. Inset: The truth table of the OR logic gate. Concentrations of DNA1/LOCK1 and DNA2/LOCK2:100 nM, H1 and H2:0.5 μM, CD33 and CD123:50 ng/mL were incubated for 55 min, followed by the addition of Cas12a/gRNA: 150 nM, FQ reporter: 1 μM. (B) Real-time fluorescence curves of CRISPR-CHA reaction in the OR logic gate. (C) Fluorescence intensity of the OR logic gate. Statistical significance was determined by *t*-test (***p < 0.001, n = 3). (D) Color reaction under blue light of the OR logic gate.

(Figure S5 and Table S2), were optimized to achieve the best analytical performance for the logic gate model.

After optimizing the conditions, we evaluated the dynamic range and sensitivity of the biosensor by testing the analytical performance for CD33 detection using the YES logic gate. Figure 2B shows the gradual increase in fluorescence signals as CD33 levels increased from 0 to 60 ng/mL. In Figure 2C The fluorescence intensity has a good linear relationship with the CD33 concentration, which increased from 10 to 50 ng/mL. The linear regression equation is $Y = 5.73 \times 10^4 X + 6.85 \times 10^5$ ($R^2 = 0.993$), where Y is the Fluorescence intensity and X is the CD33 concentration. Based on 3S/N, the limit of detection is 0.1 ng/mL.

The YES logic gate model is a versatile bioanalytical method. When different target molecules are introduced, it only requires the substitution of different aptamer sequences, while the CHA circuit and CRISPR-related components remain unchanged. To verify the approach's applicability, we used CD123 as a test target to construct the YES gate (Figure 3A,B,D, sequences are given in Table S3). We also performed a 2 × 2 orthogonality experiment for CD33 and CD123, demonstrating their specificity and noninterference (Figure 3C). This work lays the groundwork for future two-input logic gates.

3.1.4. Analysis of CD33 in the Serum Sample. To assess the stability of the logic gate model in complex sample environments, we conducted YES gate detection of CD33 in human healthy serum. The real-time fluorescence curves of the CRISPR system and CHA reaction mixture are shown in Figure 2D, while the final fluorescence intensity of the logic gate is presented in Figure 2E. The differences in the samples can be clearly distinguished when the reaction tubes are placed under blue light, as shown in Figure 2F. We also tested the feasibility of the logic gates at lower concentrations and found that the detection limit in serum samples was 0.5 ng/mL (Figure S6A), which is comparable to the results obtained in CHA buffer (0.1 ng/mL). These findings demonstrate that the matrix in serum has a minimal impact on the performance of the logic gate. We spiked serum with various concentrations of CD33 to determine the linear range of the YES logic gate in a serum environment. The experimental results are shown in Figure S6B. In 50% healthy human serum, CD33 concentrations of 40, 30, and 20 ng/mL were tested. The recovery rates ranged from 93.72 to 108.47%, with relative standard deviations (RSD) between 2.73 and 5.50%, as shown in Table 1. These results indicate that the logic gate biosensor holds potential for practical applications, as the complex sample matrix does not affect the analytical performance of the logic system.

https://doi.org/10.1021/acsomega.5c00660
ACS Omega 2025, 10, 13634−13644

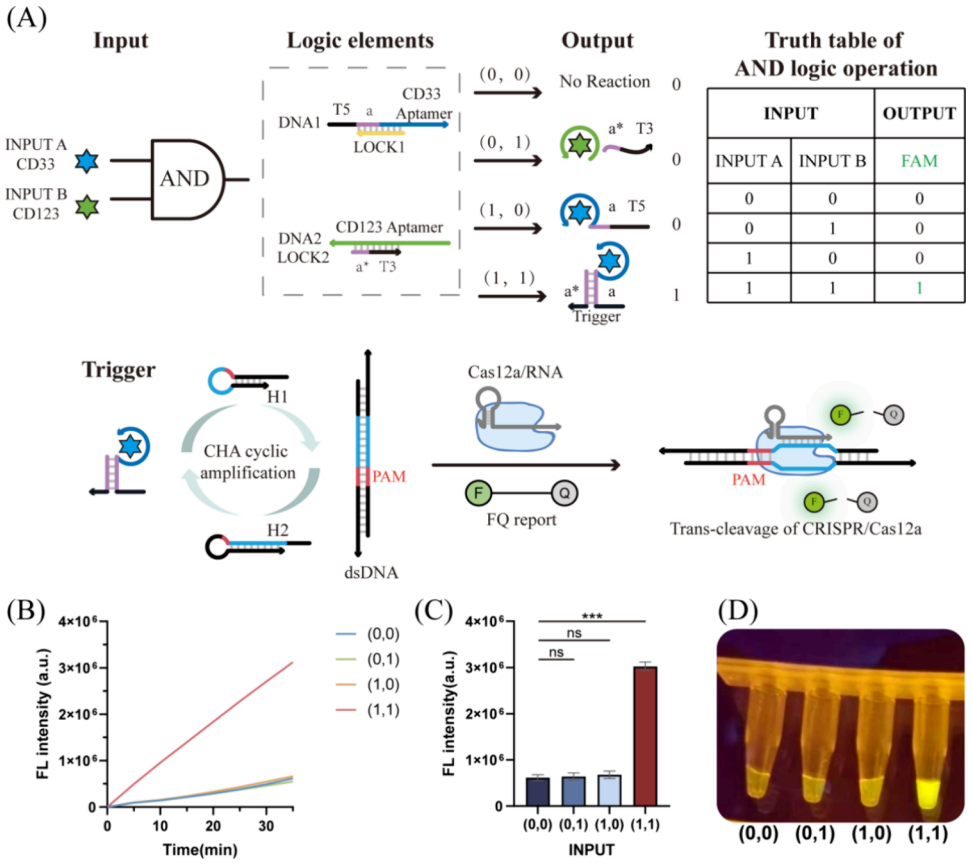

Figure 5. Operating principle and experimental results of the AND logic gate: (A) Schematic illustration of the AND logic gate using CD33 and CD123 as inputs. Inset: The truth table of the AND logic gate. Concentrations of DNA1/LOCK1 and DNA2/LOCK2:100 nM, H1 and H2:0.5 μM, CD33 and CD123:50 ng/mL were incubated for 55 min, followed by the addition of Cas12a/gRNA: 150 nM, FQ reporter: 1 μM. (B) Real-time fluorescence curves of CRISPR-CHA reaction in AND logic gate. (C) Fluorescence intensity of AND logic gate. Statistical significance was determined by t test (***$p < 0.001$, ns not significant, $n = 3$). (D) Color reaction under blue light of the AND logic gate.

3.2. Logic Gate Biosensing Platform for the Detection. *3.2.1. OR Logic Gate.* We also constructed an OR logic gate using CD33 and CD123 as dual inputs, where CD33 and CD123 were defined as inputs A and B, respectively. The corresponding Trigger DNA and aptamer sequences are clearly listed in Table S4. Additionally, Figure 4A illustrates the truth table for the OR logic gate, demonstrating its logical operations.

In the absence of inputs (0,0), the toehold domain trigger in DNA1 and DNA2 remains inaccessible, preventing any self-assembly reaction. As a result, only a minimal fluorescence signal is observed (output = 0). When input A (1,0) is introduced, it interacts with DNA1, releasing LOCK1. This enables DNA1 to initiate the assembly of H1 and H2 into the H1/H2 double-stranded DNA (dsDNA), similar to the mechanism of the YES logic gate. The subsequent recognition by the Cas12a/gRNA complex leads to the cleavage of ssDNA-FQ, generating a strong fluorescence signal (output = 1). In the presence of input B (0,1), the Trigger domain of DNA2 is released, initiating strand displacement and producing dsDNA containing the target sequence for Cas12a/gRNA. This process also results in a highly fluorescent signal (output = 1). When both inputs A and B are present (1,1), DNA1 and DNA2 are simultaneously unblocked, allowing the cleavage and self-assembly reactions to occur concurrently. This dual activation produces an amplified fluorescence signal (output = 1).

Figure 4B presents the real-time fluorescence curve of the CRISPR-CHA reaction for the OR logic gate. The final fluorescence intensity for the OR logic gate, shown in Figure 4C, reveals a statistically significant difference between the presence and absence of the output ($p < 0.001$, $n = 3$). The colorimetric signal of the OR logic gate is displayed in Figure 4D. The OR logic gate produces high response signals (output = 1) for the input combinations (1,0), (0,1), and (1,1), demonstrating its computational functionality.

3.2.2. AND Logic Gate. Additionally, we constructed an AND logic gate with Figure 5A illustrating its design principle and truth table. The corresponding DNA and RNA sequences are clearly listed in Table S5, where CD33 and CD123 were defined as input A and input B, respectively.

When the logic gate lacks a target (0,0), no reaction occurs, resulting in an output of 0. In the presence of input B (0,1), LOCK2 is released but the free LOCK2 does not contain the complete Trigger DNA sequence, preventing the opening of hairpin H1. Consequently, the output remains 0. When input A (1,0) is introduced, the block on DNA1 is removed. However, DNA1 lacks the T3 domain and contains only the T5 domain. For the toehold-mediated strand displacement reaction to open hairpin H1, both the T3 and T5 domains must be present in close proximity within the Trigger DNA. Since this condition is not met, the self-assembly reaction between H1 and H2 cannot proceed, leading to an output of 0.

https://doi.org/10.1021/acsomega.5c00660
ACS Omega 2025, 10, 13634−13644

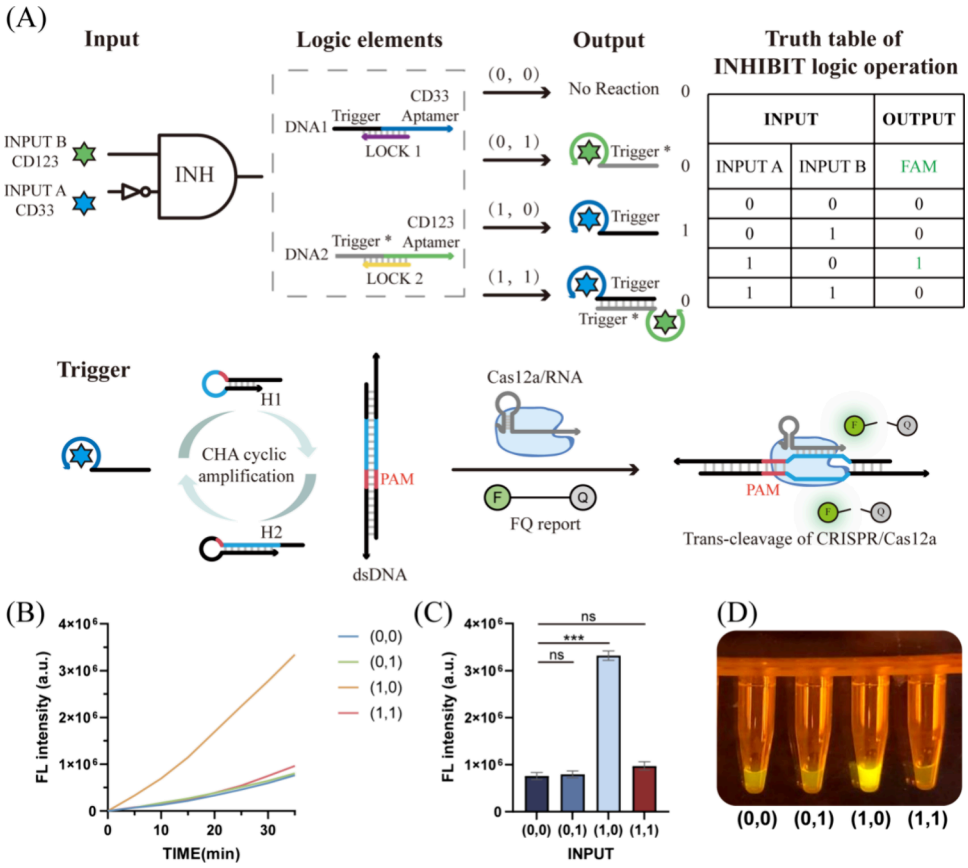

Figure 6. Operating principle and experimental results of INHIBIT logic gate: (A) Schematic illustration of the INHIBIT logic gate using CD33 and CD123 as inputs. Inset: The truth table of the INHIBIT logic gate. Concentrations of DNA1/LOCK1 and DNA2/LOCK2:100 nM, H1 and H2:0.5 μM, CD33 and CD123:50 ng/mL were incubated for 55 min, followed by the addition of Cas12a/gRNA: 150 nM, FQ reporter: 1 μM. (B) Real-time fluorescence curves of CRISPR-CHA reaction in INHIBIT logic gate. (C) Fluorescence intensity of INHIBIT logic gate. Statistical significance was determined by t test (***$p < 0.001$, ns not significant, $n = 3$). (D) Color reaction under blue light of the INHIBIT logic gate.

When both inputs A and B are present (1,1), the released LOCK2 hybridizes with the opened DNA1 through a−a* binding, forming the complete Trigger DNA. This intact Trigger DNA initiates the toehold-mediated strand displacement reaction, opening hairpin H1. Subsequently, H1 and H2 undergo cyclic assembly, generating a large quantity of H1/H2 double-stranded DNA (dsDNA). Upon recognition by the Cas12a/gRNA complex, the ssDNA-FQ reporter is cleaved, producing a strong fluorescent signal (output = 1).

The colorimetric signal of the AND logic gate is displayed in Figure 5D. Figure 5B presents the real-time fluorescence curve of the CRISPR-CHA reaction for the AND logic gate. The final fluorescence intensity for the AND logic gate, shown in Figure 5C, demonstrates a statistically significant difference between the presence and absence of the output ($p < 0.001$, $n = 3$). To validate the feasibility of the logic gate at lower concentrations, we selected the AND gate as a representative for analysis in serum samples at a relatively low input concentration (20 ng/mL), with the results shown in Figure S7. Only the input combination (1,1) can result in a 1 in an AND logic gate calculation; Other input combinations (0,0), (1,0), and (0,1) result in 0.

3.2.3. INHIBIT Logic Gate. An INHIBIT logic gate was constructed using CD33 and CD123 as inputs, as illustrated in Figure 6A, along with its corresponding truth table. The oligonucleotide sequences are clearly listed in Table S6.

In the absence of a target (0,0), the logic gate model produces no response, resulting in an output of 0. When input A (1,0) is introduced, the unblocked Trigger domain in DNA1 initiates the self-assembly of H1 and H2, forming H1/H2 double-stranded DNA (dsDNA). This dsDNA is recognized by the Cas12a/gRNA complex, leading to the cleavage of the FQ reporter and generating a strong fluorescent signal (output = 1). In the presence of input B (0,1), LOCK2 does not block DNA2, but DNA2 lacks the Trigger domain required for toehold-mediated strand displacement. As a result, the output remains 0. When both inputs A and B are present simultaneously (1,1), released DNA1 binds to DNA2 through Trigger−Trigger* base complementarity. This interaction prevents the self-assembly of H1 and H2, resulting in an output of 0.

Figure 6B presents the real-time fluorescence curve of the CRISPR-CHA reaction for the INHIBIT logic gate. The final fluorescence intensity for the INHIBIT logic gate is shown in Figure 6C. A statistically significant difference ($p < 0.001$, $n = 3$) was observed between the presence and absence of the output. The colorimetric signal of the INHIBIT logic gate is depicted in Figure 6D. In the INHIBIT logic gate, the output is calculated as 1 only when the input is (1,0); otherwise, the output is 0.

3.2.4. NOR Logic Gate. Furthermore, a NOR logic gate was developed, with its design principle and truth table illustrated in Figure 7A. Inputs A and B were defined as CD33 and

https://doi.org/10.1021/acsomega.5c00660
ACS Omega 2025, 10, 13634−13644

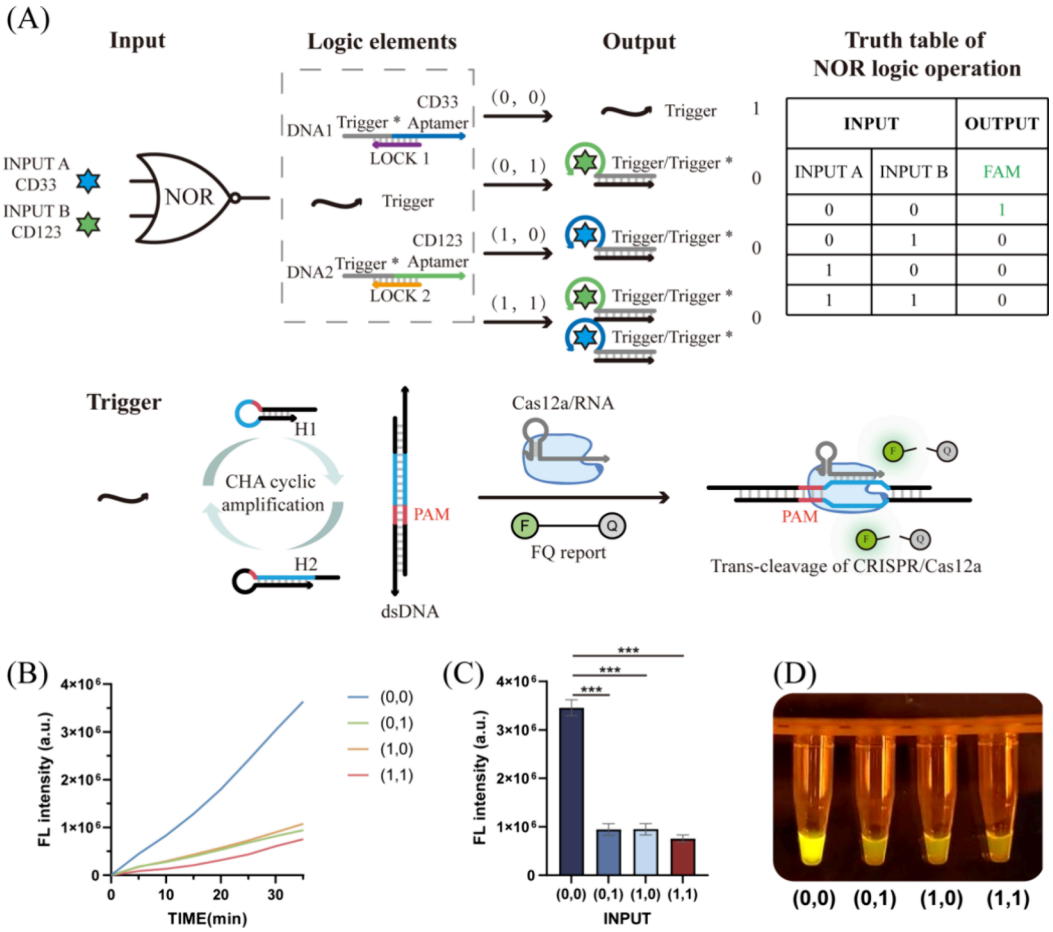

Figure 7. Operating principle and experimental results of the NOR logic gate: (A) Schematic illustration of the NOR gate using CD33 and CD123 as inputs. Inset: The truth table of the NOR logic gate. Concentrations of 80 nM Trigger, DNA1/LOCK1 and DNA2/LOCK2:100 nM, H1 and H2:0.5 μM, CD33 and CD123:50 ng/mL were incubated for 55 min, followed by the addition of Cas12a/gRNA: 150 nM, FQ reporter: 1 μM. (B) Real-time fluorescence curves of CRISPR-CHA reaction in NOR logic gate. (C) Fluorescence intensity of NOR logic gate. Statistical significance was determined by t test (***$p < 0.001$, $n = 3$). (D) Color reaction under blue light of the NOR logic gate.

CD123, respectively. The sequences of the Trigger DNA and aptamers are explicitly outlined in Table S7. The reaction is governed by a hairpin structure, which initiates a strand displacement process upon introduction of a free Trigger into the system. Considering that the NOR gate involves more components than other logic gates, we have included a detailed logic operation of the NOR gate in the Supporting Information Figure S8.

In the absence of inputs (0,0), the Trigger initiates the assembly reaction between H1 and H2, generating H1/H2 double-stranded DNA (dsDNA) and producing a strong fluorescent signal (output = 1). When either input A (1,0) or input B (0,1) is present, the addition of CD33 or CD123 releases LOCK1 or LOCK2, respectively, activating the toehold domain Trigger*. Through complementary base pairing, released DNA1 or DNA2 binds to the free Trigger in the system, preventing the self-assembly of H1 and H2. As a result, the output in these states is 0. When both inputs A and B are present simultaneously (1,1), DNA1 and DNA2 are unblocked and the exposed domain Trigger* once again binds to the free Trigger, inhibiting the assembly reaction. Consequently, the output remains 0.

Figure 7B presents the real-time fluorescence curve of the CRISPR-CHA reaction for the NOR logic gate. The final fluorescence intensity for the NOR logic gate is shown in Figure 7C, while Figure 7D displays its colorimetric signal. A significant difference ($p < 0.001$, $n = 3$) was observed between the presence and absence of output. In the NOR logic gate, only the input (0,0) yields an output of 1; all other combinations (1,1), (1,0), and (0,1) result in 0.

3.3. Discussion and Conclusions. As demonstrated by our research, we have successfully fabricated a universal molecular logic gate biosensing platform based on CRISPR-Cas12a and hairpin probes that contain nucleic acid aptamers, expanding the range of input types. By using CHA and CRISPR, we achieved signal transduction and amplification, so that fluorescent signals could serve as the outcomes of logical operations. The reaction between the antigen and the aptamer sequence releases the DNA domain Trigger. Trigger can open hairpin H1 and initiate the self-assembly process of the two hairpin DNA probes. Through cyclic strand displacement in DNA circuits, the formed dsDNA products containing the PAM sequence can be recognized by CRISPR-Cas12a with crRNA. Activated Cas12a can cleave FAM-BHQ-modified ssDNA, generating a high fluorescence signal for target monitoring. Through the rational design of DNA probes, we constructed a biosensor logic platform that includes YES, OR, NOR, and INHIBIT logic gates, enhancing the performance of the biosensor in complex environments and making it suitable for various analytical needs.

https://doi.org/10.1021/acsomega.5c00660
ACS Omega 2025, 10, 13634−13644

Our molecular logic gate model exhibits significant advantages in stability, sensitivity, response temperature, signal visualization, detection range, and response time. Unlike traditional nucleic acid−based models,[29,48] our system achieves multitarget recognition by modifying aptamer sequences, leveraging their high affinity and specificity for target molecules. This flexibility allows the detection of diverse inputs (e.g., proteins, heavy metals, and pathogens), making it highly applicable in food safety, environmental monitoring, and disease diagnosis. Notably, our model operates effectively at 25 °C, eliminating the need for high-temperature environments.[40,49] Compared to sensors requiring complex equipment like spectrophotometers,[42,50] our model uses a portable blue light panel for direct signal visualization, reducing costs and improving convenience for on-site detection. By combining CHA and CRISPR-Cas12a for synergistic signal amplification, our system achieves high sensitivity and specificity, with minimal nontarget interference. In CD33 detection, our model achieves a detection limit of 0.1 ng/mL (S/N = 3), comparable to existing biosensors but with faster reaction times and simpler operation,[5] as highlighted in Table S8. To address DNase interference in serum, samples were pretreated based on established biosensor protocols,[5] ensuring reliable logic gate operation. In spiked serum samples, the biosensor demonstrated a detection limit of 0.5 ng/mL for target biomarkers, achieving sensitivity comparable to that of commercial ELISA kits (typically 1.5−50 ng/mL). Notably, the platform maintains this high sensitivity (0.5 ng/mL) while offering distinct advantages over traditional methods: (1) a 57% reduction in assay time (from >3.5 to <1.5 h), and (2) the elimination of the need for specialized microplate readers. The successful detection of target biomarkers at concentrations comparable to those achieved by commercial kits in complex biological matrices confirms the potential of this system for point-of-care diagnostics and therapeutic monitoring.

Despite these advantages, challenges remain in complex sample detection due to potential interference. Future work should optimize sample pretreatment and address scalability and cost issues. Expanding the detection range to include environmental pollutants, heavy metals, and pathogens, alongside integration with technologies like microfluidics and the lateral flow assay (LFA), could further enhance its applications in food safety, environmental monitoring, and early disease diagnosis.

■ ASSOCIATED CONTENT

Data Availability Statement

Data will be made available on request.

Supporting Information

The Supporting Information is available free of charge at https://pubs.acs.org/doi/10.1021/acsomega.5c00660.

Oligonucleotides sequences (Tables S1−S7), electrophoretic analysis of different logic gates (Figure S1), selectivity and feasibility investigation (Figure S2), optimization of experimental parameters (Figures S3−S5), sensitivity of the YES logic gate in serum and the linear range for CD33 analysis in serum sample (Figure S6), fluorescence intensity of the AND logic gate in serum (Figure S7), detailed logic operation of the NOR logic gate (Figure S8), and comparison of the biosensors for disease antigen detection (Table S8) (PDF)

■ AUTHOR INFORMATION

Corresponding Authors

Fengyue Zhang − *Institute of Medical Artificial Intelligence, Binzhou Medical University, Yantai 264003 Shandong, PR China; College of Life Science, Beijing Institute of Technology, Beijing 100081, PR China*; Email: fyzhang@bit.edu.cn

Bo Liu − *Institute of Medical Artificial Intelligence, Binzhou Medical University, Yantai 264003 Shandong, PR China*; Email: liubo@bzmc.edu.cn

Authors

Xinyi Yang − *Institute of Medical Artificial Intelligence, Binzhou Medical University, Yantai 264003 Shandong, PR China*; orcid.org/0009-0006-5726-480X

Xiaolong Shi − *Institution of Computational Science and Technology, Guangzhou University, Guangzhou 510006 Guangdong, PR China*

Chenyu Lv − *Institute of Medical Artificial Intelligence, Binzhou Medical University, Yantai 264003 Shandong, PR China*

Wenbin Liu − *Institution of Computational Science and Technology, Guangzhou University, Guangzhou 510006 Guangdong, PR China*; orcid.org/0000-0001-9091-3177

Complete contact information is available at: https://pubs.acs.org/10.1021/acsomega.5c00660

Funding

This work was supported in part by the National Natural Science Foundation of China (nos. 62272061 and 62272060), the earmarked fund for Binzhou Medical University.

Notes

The authors declare no competing financial interest.

■ ACKNOWLEDGMENTS

We thank Dr. Lili Ren from Science and Technology Research Center of China Customs and Dr. Chongjian Chen and Dr Xuejia Cheng from SynsorBio Technology Co., Ltd., for providing technical assistance.

■ ABBREVIATIONS

AML	acute myeloid leukemia
CRISPR	clustered regularly interspaced short palindromic repeats
Cas	CRISPR-associated
gRNA	guide RNA
CHA	catalytic hairpin assembly
SELEX	systematic evolution of ligands by exponential enrichment
PAM	protospacer adjacent motif
dsDNA	double-stranded DNA
ssDNA	single-stranded DNA
PCR	polymerase chain reaction
DNA	deoxyribonucleic acid
PBS	phosphate buffered saline
HPLC	high performance liquid chromatography
DEPC	diethyl pyrocarbonate
RSD	relative standard deviation

■ REFERENCES

(1) Erbas-Cakmak, S.; Kolemen, S.; Sedgwick, A. C.; Gunnlaugsson, T.; James, T. D.; Yoon, J.; Akkaya, E. U. Molecular Logic Gates: The Past, Present and Future. *Chem. Soc. Rev.* **2018**, *47* (7), 2228−2248.

(2) Chen, X.; Liu, X.; Wang, F.; Li, S.; Chen, C.; Qiang, X.; Shi, X. Massively Parallel DNA Computing Based on Domino DNA Strand Displacement Logic Gates. *ACS Synth. Biol.* **2022**, *11* (7), 2504−2512.
(3) Li, W.; Yang, Y.; Yan, H.; Liu, Y. Three-Input Majority Logic Gate and Multiple Input Logic Circuit Based on DNA Strand Displacement. *Nano Lett.* **2013**, *13* (6), 2980−2988.
(4) Qian, L.; Winfree, E. Scaling Up Digital Circuit Computation with DNA Strand Displacement Cascades. *Science* **2011**, *332* (6034), 1196−1201.
(5) Gao, R.; Ji, R.; Dong, W. Catalytic Hairpin Assembly-Assisted Dual-Signal Amplification Platform for Ultrasensitive Detection of Tumor Markers and Intelligent Diagnosis of Gastric Cancer. *Talanta* **2023**, *265*, No. 124812.
(6) Xing, Y.; Li, X.; Yuan, T.; Cheng, W.; Li, D.; Yu, T.; Ding, X.; Ding, S. Engineering High-Performance Hairpin Stacking Circuits for Logic Gate Operation and Highly Sensitive Biosensing Assay of microRNA. *Analyst* **2017**, *142* (24), 4834−4842.
(7) Elbaz, J.; Lioubashevski, O.; Wang, F.; Remacle, F.; Levine, R. D.; Willner, I. DNA Computing Circuits Using Libraries of DNAzyme Subunits. *Nat. Nanotechnol* **2010**, *5* (6), 417−422.
(8) Pan, J.; Deng, F.; Liu, Z.; Shi, G.; Chen, J. Toehold-Mediated Cascade Catalytic Assembly for Mycotoxin Detection and Its Logic Applications. *Anal. Chem.* **2022**, *94* (8), 3693−3700.
(9) Stojanovic, M. N.; Stefanovic, D. A Deoxyribozyme-Based Molecular Automaton. *Nat. Biotechnol.* **2003**, *21* (9), 1069−1074.
(10) Zeng, Z.; Roobrouck, A.; Deschamps, G.; Bonnevaux, H.; Guerif, S.; De Brabandere, V.; Amara, C.; Dejonckheere, E.; Virone-Oddos, A.; Chiron, M.; Konopleva, M.; Dullaers, M. Dual-Targeting CD33/CD123 NANOBODY T-Cell Engager with Potent Anti-AML Activity and Good Safety Profile. *Blood Adv.* **2024**, *8* (9), 2059−2073.
(11) Abdollahpour-Alitappeh, M.; Razavi-Vakhshourpour, S.; Abolhassani, M. Development of a New anti-CD123 Monoclonal Antibody to Target the Human CD123 Antigen as an Acute Myeloid Leukemia Cancer Stem Cell Biomarker. *Biotechnol. Appl. Biochem.* **2018**, *65* (6), 841−847.
(12) El Achi, H.; Dupont, E.; Paul, S.; Khoury, J. D. CD123 as a Biomarker in Hematolymphoid Malignancies: Principles of Detection and Targeted Therapies. *Cancers* **2020**, *12* (11), 3087.
(13) Eckel, A. M.; Cherian, S.; Miller, V.; Soma, L. CD33 Expression on Natural Killer Cells Is a Potential Confounder for Residual Disease Detection in Acute Myeloid Leukemia by Flow Cytometry. *Cytometry, Part B* **2020**, *98* (2), 174−178.
(14) Wißfeld, J.; Mathews, M.; Mossad, O.; Picardi, P.; Cinti, A.; Redaelli, L.; Pradier, L.; Brüstle, O.; Neumann, H. Reporter Cell Assay for Human CD33 Validated by Specific Antibodies and Human iPSC-Derived Microglia. *Sci. Rep.* **2021**, *11* (1), 13462.
(15) Yang, C.; Wang, Y.; Ge, M. H.; Fu, Y. J.; Hao, R.; Islam, K.; Huang, P.; Chen, F.; Sun, J.; Hong, D. F.; Naranmandura, H. Rapid Identification of Specific DNA Aptamers Precisely Targeting CD33 Positive Leukemia Cells through a Paired Cell-Based Approach. *Biomater. Sci.* **2019**, *7* (3), 938−950.
(16) Wu, H.; Wang, M.; Dai, B.; Zhang, Y.; Yang, Y.; Li, Q.; Duan, M.; Zhang, X.; Wang, X.; Li, A.; Zhang, L. Novel CD123-Aptamer-Originated Targeted Drug Trains for Selectively Delivering Cytotoxic Agent to Tumor Cells in Acute Myeloid Leukemia Theranostics. *Drug Delivery* **2017**, *24* (1), 1216−1229.
(17) Wang, M.; Wu, H.; Duan, M.; Yang, Y.; Wang, G.; Che, F.; Liu, B.; He, W.; Li, Q.; Zhang, L. SS30, a Novel Thioaptamer Targeting CD123, Inhibits the Growth of Acute Myeloid Leukemia Cells. *Life Sci.* **2019**, *232*, No. 116663.
(18) Tuerk, C.; Gold, L. Systematic Evolution of Ligands by Exponential Enrichment: RNA Ligands to Bacteriophage T4 DNA Polymerase. *Science* **1990**, *249* (4968), 505−510.
(19) Jayasena, S.; Aptamers, D. An Emerging Class of Molecules That Rival Antibodies in Diagnostics. *Clin. Chem.* **1999**, *45* (9), 1628−1650.
(20) Mairal, T.; Cengiz Özalp, V.; Lozano Sánchez, P.; Mir, M.; Katakis, I.; O'Sullivan, C. K. Aptamers: Molecular Tools for Analytical Applications. *Anal. Bioanal. Chem.* **2008**, *390* (4), 989−1007.
(21) Dunn, M. R.; Jimenez, R. M.; Chaput, J. C. Analysis of Aptamer Discovery and Technology. *Nat. Rev. Chem.* **2017**, *1* (10), No. 0076.
(22) Wu, L.; Wang, Y.; Xu, X.; Liu, Y.; Lin, B.; Zhang, M.; Zhang, J.; Wan, S.; Yang, C.; Tan, W. Aptamer-Based Detection of Circulating Targets for Precision Medicine. *Chem. Rev.* **2021**, *121* (19), 12035−12105.
(23) Ma, X.; Suo, T.; Zhao, F.; Shang, Z.; Chen, Y.; Wang, P.; Li, B. Integrating CRISPR/Cas12a with Strand Displacement Amplification for the Ultrasensitive Aptasensing of Cadmium(II). *Anal. Bioanal. Chem.* **2023**, *415* (12), 2281−2289.
(24) Yin, P.; Choi, H. M. T.; Calvert, C. R.; Pierce, N. A. Programming Biomolecular Self-Assembly Pathways. *Nature* **2008**, *451* (7176), 318−322.
(25) Jiang, Y. S.; Bhadra, S.; Li, B.; Ellington, A. D. Mismatches Improve the Performance of Strand-Displacement Nucleic Acid Circuits. *Angew. Chem., Int. Ed.* **2014**, *53* (7), 1845−1848.
(26) Karunanayake Mudiyanselage, A. P. K. K.; Yu, Q.; Leon-Duque, M. A.; Zhao, B.; Wu, R.; You, M. Genetically Encoded Catalytic Hairpin Assembly for Sensitive RNA Imaging in Live Cells. *J. Am. Chem. Soc.* **2018**, *140* (28), 8739−8745.
(27) Chen, P.; Wang, L.; Qin, P.; Yin, B.-C.; Ye, B.-C. An RNA-Based Catalytic Hairpin Assembly Circuit Coupled with CRISPR-Cas12a for One-Step Detection of microRNAs. *Biosens. Bioelectron.* **2022**, *207*, No. 114152.
(28) Wu, C.; Cansiz, S.; Zhang, L.; Teng, I.-T.; Qiu, L.; Li, J.; Liu, Y.; Zhou, C.; Hu, R.; Zhang, T.; Cui, C.; Cui, L.; Tan, W. A Nonenzymatic Hairpin DNA Cascade Reaction Provides High Signal Gain of mRNA Imaging inside Live Cells. *J. Am. Chem. Soc.* **2015**, *137* (15), 4900.
(29) Zhou, Y.; Tang, L.; Lyu, J.; Shiyi, L.; Liu, Q.; Pang, R.; Li, W.; Guo, X.; Zhong, X.; He, H. A Dual Signal Amplification System with Specific Signal Identification for Rapid and Sensitive Detection of miRNA. *Talanta* **2024**, *266*, No. 125097.
(30) Knott, G. J.; Doudna, J. A. CRISPR-Cas Guides the Future of Genetic Engineering. *Science* **2018**, *361* (6405), 866−869.
(31) Pickar-Oliver, A.; Gersbach, C. A. The next Generation of CRISPR−Cas Technologies and Applications. *Nat. Rev. Mol. Cell Biol.* **2019**, *20* (8), 490−507.
(32) Tang, Y.; Gao, L.; Feng, W.; Guo, C.; Yang, Q.; Li, F.; Le, X. C. The CRISPR−Cas Toolbox for Analytical and Diagnostic Assay Development. *Chem. Soc. Rev.* **2021**, *50* (21), 11844−11869.
(33) Cox, D. B. T.; Gootenberg, J. S.; Abudayyeh, O. O.; Franklin, B.; Kellner, M. J.; Joung, J.; Zhang, F. RNA Editing with CRISPR-Cas13. *Science* **2017**, *358* (6366), 1019−1027.
(34) Abudayyeh, O. O.; Gootenberg, J. S.; Essletzbichler, P.; Han, S.; Joung, J.; Belanto, J. J.; Verdine, V.; Cox, D. B. T.; Kellner, M. J.; Regev, A.; Lander, E. S.; Voytas, D. F.; Ting, A. Y.; Zhang, F. RNA Targeting with CRISPR−Cas13. *Nature* **2017**, *550* (7675), 280−284.
(35) Li, S.-Y.; Cheng, Q.-X.; Liu, J.-K.; Nie, X.-Q.; Zhao, G.-P.; Wang, J. CRISPR-Cas12a Has Both Cis- and Trans-Cleavage Activities on Single-Stranded DNA. *Cell Res.* **2018**, *28* (4), 491−493.
(36) Sam, I. K.; Chen, Y.; Ma, J.; Li, S.; Ying, R.; Li, L.; Ji, P.; Wang, S.; Xu, J.; Bao, Y.; Zhao, G.; Zheng, H.; Wang, J.; Sha, W.; Wang, Y. TB-QUICK: CRISPR-Cas12b-Assisted Rapid and Sensitive Detection of Mycobacterium Tuberculosis. *J. Infect.* **2021**, *83* (1), 54−60.
(37) Harrington, L. B.; Burstein, D.; Chen, J. S.; Paez-Espino, D.; Ma, E.; Witte, I. P.; Cofsky, J. C.; Kyrpides, N. C.; Banfield, J. F.; Doudna, J. A. Programmed DNA Destruction by Miniature CRISPR-Cas14 Enzymes. *Science* **2018**, *362* (6416), 839−842.
(38) Fonfara, I.; Richter, H.; Bratovič, M.; Le Rhun, A.; Charpentier, E. The CRISPR-Associated DNA-Cleaving Enzyme Cpf1 Also Processes Precursor CRISPR RNA. *Nature* **2016**, *532* (7600), 517−521.
(39) Chen, J. S.; Ma, E.; Harrington, L. B.; Da Costa, M.; Tian, X.; Palefsky, J. M.; Doudna, J. A. CRISPR-Cas12a Target Binding

https://doi.org/10.1021/acsomega.5c00660
ACS Omega 2025, 10, 13634−13644

Unleashes Indiscriminate Single-Stranded DNase Activity. *Science* **2018**, *360* (6387), 436−439.
(40) Peng, S.; Tan, Z.; Chen, S.; Lei, C.; Nie, Z. Integrating CRISPR-Cas12a with a DNA Circuit as a Generic Sensing Platform for Amplified Detection of microRNA. *Chem. Sci.* **2020**, *11* (28), 7362−7368.
(41) Gong, S.; Wang, X.; Zhou, P.; Pan, W.; Li, N.; Tang, B. AND Logic-Gate-Based CRISPR/Cas12a Biosensing Platform for the Sensitive Colorimetric Detection of Dual miRNAs. *Anal. Chem.* **2022**, *94* (45), 15839−15846.
(42) Yan, C.; Shi, G.; Chen, J. Fluorescent Detection of Two Pesticides Based on CRISPR-Cas12a and Its Application for the Construction of Four Molecular Logic Gates. *J. Agric. Food Chem.* **2022**, *70* (39), 12700−12707.
(43) Ding, X.; Yin, K.; Li, Z.; Lalla, R. V.; Ballesteros, E.; Sfeir, M. M.; Liu, C. Ultrasensitive and Visual Detection of SARS-CoV-2 Using All-in-One Dual CRISPR-Cas12a Assay. *Nat. Commun.* **2020**, *11* (1), 4711.
(44) Jiang, Y.; Hu, M.; Liu, A.-A.; Lin, Y.; Liu, L.; Yu, B.; Zhou, X.; Pang, D.-W. Detection of SARS-CoV-2 by CRISPR/Cas12a-Enhanced Colorimetry. *ACS Sens.* **2021**, *6* (3), 1086−1093.
(45) Chen, J.; Shi, G.; Yan, C. Visual Test Paper for On-Site Polychlorinated Biphenyls Detection and Its Logic Gate Applications. *Anal. Chem.* **2021**, *93* (46), 15438−15444.
(46) Low, S. J.; O'Neill, M. T.; Kerry, W. J.; Krysiak, M.; Papadakis, G.; Whitehead, L. W.; Savic, I.; Prestedge, J.; Williams, L.; Cooney, J. P.; Tran, T.; Lim, C. K.; Caly, L.; Towns, J. M.; Bradshaw, C. S.; Fairley, C.; Chow, E. P. F.; Chen, M. Y.; Pellegrini, M.; Pasricha, S.; Williamson, D. A. Rapid Detection of Monkeypox Virus Using a CRISPR-Cas12a Mediated Assay: A Laboratory Validation and Evaluation Study. *Lancet Microbe* **2023**, *4*, No. e800.
(47) Chen, J.; Shi, G.; Yan, C. Portable Biosensor for On-Site Detection of Kanamycin in Water Samples Based on CRISPR-Cas12a and an off-the-Shelf Glucometer. *Sci. Total Environ.* **2023**, *872*, No. 162279.
(48) Oesinghaus, L.; Simmel, F. C. Switching the Activity of Cas12a Using Guide RNA Strand Displacement Circuits. *Nat. Commun.* **2019**, *10* (1), 2092.
(49) Jia, H.-Y.; Zhao, H.-L.; Wang, T.; Chen, P.-R.; Yin, B.-C.; Ye, B.-C. A Programmable and Sensitive CRISPR/Cas12a-Based MicroRNA Detection Platform Combined with Hybridization Chain Reaction. *Biosens. Bioelectron.* **2022**, *211*, No. 114382.
(50) Wang, N.; Jiang, Y.; Nie, K.; Li, D.; Liu, H.; Wang, J.; Huang, C.; Li, C. Toehold-Mediated Strand Displacement Reaction-Propelled Cascade DNAzyme Amplifier for microRNA Let-7a Detection. *Chin. Chem. Lett.* **2023**, *34* (6), No. 107906.

https://doi.org/10.1021/acsomega.5c00660
ACS Omega 2025, 10, 13634−13644